

RESEARCH ARTICLE

Reciprocal interaction between I_{K1} and I_f in biological pacemakers: A simulation studyYacong Li¹, Kuanquan Wang^{1*}, Qince Li^{1,2}, Jules C. Hancox^{3,4}, Henggui Zhang^{2,4,5*}

1 School of Computer Science and Technology, Harbin Institute of Technology, Harbin, China, **2** Peng Cheng Laboratory, Shenzhen, China, **3** School of Physiology, Pharmacology and Neuroscience, Medical Sciences Building, University Walk, Bristol, United Kingdom, **4** Biological Physics Group, School of Physics and Astronomy, The University of Manchester, Manchester, United Kingdom, **5** Key Laboratory of Medical Electrophysiology of Ministry of Education and Medical Electrophysiological Key Laboratory of Sichuan Province, Institute of Cardiovascular Research, Southwest Medical University, Luzhou, China

* wangkq@hit.edu.cn (KW); henggui.zhang@manchester.ac.uk (HZ)



OPEN ACCESS

Citation: Li Y, Wang K, Li Q, Hancox JC, Zhang H (2021) Reciprocal interaction between I_{K1} and I_f in biological pacemakers: A simulation study. *PLoS Comput Biol* 17(3): e1008177. <https://doi.org/10.1371/journal.pcbi.1008177>

Editor: Jeffrey J. Saucerman, University of Virginia, UNITED STATES

Received: July 17, 2020

Accepted: February 17, 2021

Published: March 10, 2021

Copyright: © 2021 Li et al. This is an open access article distributed under the terms of the [Creative Commons Attribution License](https://creativecommons.org/licenses/by/4.0/), which permits unrestricted use, distribution, and reproduction in any medium, provided the original author and source are credited.

Data Availability Statement: All relevant data are within the manuscript and its [Supporting Information](#) files.

Funding: This research was partially funded by research grants from Engineering and Physical Sciences Research Council (EP/J00958X/1; EP/I029826/1 to HZ). The funders had no role in study design, data collection and analysis, decision to publish, or preparation of the manuscript.

Competing interests: The authors have declared that no competing interests exist.

Abstract

Pacemaking dysfunction (PD) may result in heart rhythm disorders, syncope or even death. Current treatment of PD using implanted electronic pacemakers has some limitations, such as finite battery life and the risk of repeated surgery. As such, the biological pacemaker has been proposed as a potential alternative to the electronic pacemaker for PD treatment. Experimentally and computationally, it has been shown that bio-engineered pacemaker cells can be generated from non-rhythmic ventricular myocytes (VMs) by knocking out genes related to the inward rectifier potassium channel current (I_{K1}) or by overexpressing hyperpolarization-activated cyclic nucleotide gated channel genes responsible for the “funny” current (I_f). However, it is unclear if a bio-engineered pacemaker based on the modification of I_{K1} - and I_f -related channels simultaneously would enhance the ability and stability of bio-engineered pacemaking action potentials. In this study, the possible mechanism(s) responsible for VMs to generate spontaneous pacemaking activity by regulating I_{K1} and I_f density were investigated by a computational approach. Our results showed that there was a reciprocal interaction between I_{K1} and I_f in ventricular pacemaker model. The effect of I_{K1} depression on generating ventricular pacemaker was mono-phasic while that of I_f augmentation was bi-phasic. A moderate increase of I_f promoted pacemaking activity but excessive increase of I_f resulted in a slowdown in the pacemaking rate and even an unstable pacemaking state. The dedicated interplay between I_{K1} and I_f in generating stable pacemaking and dysrhythmias was evaluated. Finally, a theoretical analysis in the I_{K1}/I_f parameter space for generating pacemaking action potentials in different states was provided. In conclusion, to the best of our knowledge, this study provides a wide theoretical insight into understandings for generating stable and robust pacemaker cells from non-pacemaking VMs by the interplay of I_{K1} and I_f , which may be helpful in designing engineered biological pacemakers for application purposes.

Author summary

Pacemaking dysfunction has become one of the most severe cardiac diseases, which may result in arrhythmia and even death. The treatment of pacemaking dysfunction by electronic pacemakers has saved millions of people in the past fifty years. However not every patient can benefit from these because of possible limitations, such as surgical implication and lack of response to the autonomic stimulus. The development of biological pacemaker based on gene engineering technology provides a promising alternative to the electronic pacemaker by manipulating the gene expression of cardiac cells. However, it is still unclear how a stable and robust biological pacemaker can be generated in this way. The present study aims to elucidate possible mechanisms responsible for a bio-engineered pacemaker using a computational electrophysiological model by modifying ionic channel properties of I_{K1} and incorporating I_f in a human ventricular cell model. Simulation results indicated that the reciprocal interaction between I_{K1} and I_f determined the stability and ability of biological pacemaker. This study provides new insight into the understanding of the initiation of pacemaking behaviours in non-rhythmic cardiac myocytes, providing a theoretical basis for experimental design of biological pacemakers.

Introduction

Currently, electronic pacemaker implantation is the only non-pharmacological therapy for some patients with pacemaking dysfunction. But electronic pacemakers have some possible limitations [1]. Implantation of a pacemaker device may have complications for patients, especially for aged ones because of their infirm health [2]. Pediatric patients can receive electronic pacemakers; however, the device has to be replaced as they grow, and repeated surgeries are needed [3]. Electronic devices can be subject to electromagnetic interference [4], which causes inconvenience to the patients. A further issue is that classical electronic pacemakers are insensitive not only to hormone stimulation [5] but also to autonomic emotion responsiveness [4], although there are some attempts to make them respond to autonomic nervous control [6]. In addition, the long-term use of electronic pacemakers has been reported to increase the risk of heart failure [7]. Appropriately designed biological pacemakers (bio-pacemakers) have the potential to overcome some of the limitations of electrical device use [8], such as the lack of pacing flexibility. Also, engineered bio-pacemakers could potentially involve only minor surgical trauma for implantation as well as facilitating chronotropic responses [9]. In previous experimental studies, it has been shown that a bio-pacemaker can be engineered *via* adenoviral gene transduction [10–12] or lentiviral vector [13,14] techniques, by which non-pacemaking cardiac myocytes (CMs) can be transformed to the rhythmic pacemaker-like cells.

The native cardiac primary pacemaker, sinoatrial node (SAN), is a special region comprised of cells with distinct electrophysiological properties to those of cells in the working myocardium. Such intrinsic and special electrophysiological properties of SAN cells are mainly manifested by their small if not absent inward rectifier potassium channel current (I_{K1}) [15], but a large “funny” current (I_f) [16] that is almost absent in atrial and ventricular cells. I_{K1} helps to hyperpolarize cell membrane potential and contributes to maintaining a stable negative resting potential in ventricular myocytes (VMs). But in the SAN, absence of I_{K1} makes a more positive maximum diastolic potential (MDP) than the resting potential in VMs, which helps its depolarization. I_f plays an important role in phase 4 depolarization of SAN action potentials, thus influences the pacemaking rate in the SAN [17]. In addition to the absence of I_{K1} and presence of I_f , T-type Ca^{2+} channel current (I_{CaT}) [18] and sustained inward current (I_{st}) [19] also

contribute to spontaneous pacemaking activity in SAN cells. Similar to I_f , I_{CaT} plays a role in the depolarization in the SAN but is usually undetectable in VMs. Such unique electrophysiological properties of SAN cells formed a theoretical basis to engineer non-pacemaking CMs into spontaneous pacemaker cells. These non-pacemaker cells include native CMs, such as ventricular [11,20–22], atrial [23] or bundle branch myocytes [24]. They can also be stem cells, such as embryonic stem cells [25–27], bone marrow stem cells [13,28,29], adipose-derived stem cells [30–32], or induced pluripotent stem cell [14,33,34].

With gene therapy, these non-rhythmic cells have been manipulated to provoke automaticity. In previous studies, knocking down the *Kir2.1* gene to reduce the expression of I_{K1} promoted spontaneous rhythms in newborn murine VMs [20]; by reprogramming the *Kir2.1* gene in guinea-pigs, VMs also produced pacemaker activity when I_{K1} was suppressed [11,21]. As I_f plays an important role in the native SAN cell pacemaking, a parallel gene therapy manipulation to create engineered bio-pacemaker has been carried out by expressing the *HCN* gene family in non-rhythmic CMs [35]. It has been shown that expressing *HCN2* produced escape beats in canine CMs [23,24] and initiated spontaneous beats in neonatal rat VMs [22]. *HCN* expression in stem cells-induced-CMs also enhanced their pacemaking rate [13,28,29,36,37]. Overexpressing *HCN4* can also induce spontaneous pacemaking activity in mouse embryonic stem cells [38]. However, acute *HCN* gene expression might have a side effect on the normal cardiac pacemaking activity [39–41]. The overexpression of the *HCN* gene in non-rhythmic CMs can cause ectopic pacemaker automaticity and even arrhythmicity [42].

It has been suggested that a combined manipulation of I_{K1} and I_f may be a better alternative for creating a bio-pacemaker [43]. The expression of the transcriptional regulator *TBX18*, which influenced both I_f and I_{K1} expression, generated appropriate automatic responses in non-pacemaking CMs [10,32,44]. In addition, reprogramming *TBX18* in porcine VMs did not show the increase of arrhythmia risk [12], indicating the probable superiority of manipulating I_{K1} and I_f jointly for generating a bio-pacemaker. Furthermore, an experimental study showed that in HEK293 cells with expression of the *Kir2.1* and the *HCN* genes, not only I_f but also moderate I_{K1} was necessary to induce spontaneous rhythmic oscillations [45].

Computational modelling offers a means to investigate different approaches to generating stable pacemaking activity. Based on the cardiac cell model, bifurcation analysis was widely used to explore the effect of changes on some individual ion channel current on the pacemaking activities, such as the role of down-regulating I_{K1} in the pacemaking initiation in VMs [46–48] and the role of I_f in the pacemaking activity in SAN cells [49]. The interplay between multiple ion channel currents in the pacemaking initiation was also investigated in VMs [50] or SAN [51] models, with focus on their roles in sustaining the spontaneous oscillation. Up to now, the dynamic interplay between I_{K1} and I_f on modulating the stability of bio-pacemaker action potentials (APs) has not yet been comprehensively investigated in biophysically detailed cardiac single-cell models.

Considering the availability of experimental data on transformation of VMs into rhythmic cells [11,20–22] and the cardiac dysfunctions arising from atrioventricular heart-block, we chose the VM cell model for investigating bio-pacemaking activity. In this study, we constructed a bio-pacemaker model based on a human VMs model [52] by manipulating I_{K1} and incorporating I_f [53] into the model. This study aimed to investigate (i) possible mechanism(s) underlying the pacemaking activity of the VMs in the I_{K1}/I_f parameter space; and (ii) the reciprocal interaction of reduced I_{K1} and increased I_f in generating stable pacemaking APs. In addition, possible factors responsible for impaired pacemaking activity due to the inappropriate ratio between I_{K1} and I_f were also investigated. Moreover, theoretical analysis of the role of I_{CaT} in I_{K1}/I_f pacemaker model was investigated. This study provides insight into generating stable and robust engineered bio-pacemaker.

Methods

Single bio-pacemaker cell model

Previous experimental studies [10,11,20–22] implemented the suppression of *Kir2.1*, the incorporation of *HCN* channels and the expression of *TBX18* to induce pacemaking in VMs. In this study, we used a human VMs model built by Ten Tusscher et al. in 2006 (TP06 model) [52] as the basal model to investigate possible pacemaking mechanisms in VM-transformed pacemaking cells. In brief, the basal VM cell model can be described by the following ordinary differential equation:

$$\frac{dV}{dt} = -\frac{I_{ion}}{C_m} \tag{1}$$

where V is the voltage across cell membrane surfaces, t is time, I_{ion} is the sum of all transmembrane ionic currents, and C_m cell capacitance.

The I_{ion} in the original ventricular model is described by the following equation:

$$I_{ion} = I_{Na} + I_{K1} + I_{to} + I_{Kr} + I_{Ks} + I_{CaL} + I_{NaCa} + I_{NaK} + I_{pCa} + I_{pK} + I_{bCa} + I_{bNa} \tag{2}$$

where I_{Na} is fast sodium channel current, I_{K1} is inward rectifier potassium channel current, I_{to} is transient outward current, I_{Kr} is rapid delayed rectifier potassium channel current, I_{Ks} is slow delayed rectifier potassium channel current, I_{CaL} is L-type calcium current, I_{NaCa} is Na^+ / Ca^{2+} exchange current, I_{NaK} is Na^+ / K^+ pump current, I_{pCa} and I_{pK} are plateau Ca^{2+} and K^+ currents, and I_{bCa} and I_{bNa} are background Ca^{2+} and Na^+ currents. The formulations and their parameters for the ionic channels of human VM cells were listed in [52,54].

To mimic the reduction of *Kir2.1* expression [11,20,21] or the suppression of I_{K1} by expressing *TBX18* [10], in simulations I_{K1} was decreased by modulating its macroscopic channel conductance (G_{K1}). To mimic the incorporation of I_f in VMs experimentally [22], we modified the basal model of Eq 2 by incorporating human SAN I_f formulation [53]. In simulations, I_f was modulated by changing its channel conductance (G_f).

As a result, the I_{ion} for the bio-pacemaker model can be described as:

$$I_{ion} = I_{Na} + I_{K1} + I_{to} + I_{Kr} + I_{Ks} + I_{CaL} + I_{NaCa} + I_{NaK} + I_{pCa} + I_{pK} + I_{bCa} + I_{bNa} + I_f \tag{3}$$

where I_{K1} could be expressed by

$$I_{K1} = S_{K1} G_{K1} \sqrt{\frac{K_o}{5.4}} x_{k1\infty} (V_m - E_k) \tag{4}$$

where G_{K1} is the conductance of I_{K1} , $x_{k1\infty}$ is a time-independent inward rectification factor, K_o is extracellular K^+ concentration and E_k is the equilibrium potentials of K^+ . S_{K1} is a scaling factor used to simulate the change of I_{K1} expression level.

The I_f channel is permeable to Na^+ and K^+ ions [53]. As a result, I_f could be described by two components:

$$I_f = I_{f,Na} + I_{f,K} \tag{5}$$

$$I_{f,Na} = S_f G_{f,Na} Y(V - E_{Na}) \tag{6}$$

$$I_{f,K} = S_f G_{f,K} Y(V - E_K) \tag{7}$$

where $G_{f,Na}$ and $G_{f,K}$ are maximal $I_{f,Na}$ and $I_{f,K}$ channel conductance, y is a time-independent inward rectification factor that is a function of voltage, E_{Na} , E_K are equilibrium potentials of

Na^+ and K^+ channels respectively, and S_f is a scaling factor used to simulate the change of I_f expression level.

Formulations of other channel currents for the VM cell model are the same as those in the original model in [52]. The bio-pacemaker cell model can be found in [S1 Code](#).

I_{CaT} was incorporated into the I_{K1}/I_f -induced bio-pacemaker cell model to investigate its role in generating pacemaking action potentials. Its formulations can be found in [50]. As a result, the I_{ion} is described as:

$$I_{ion} = I_{Na} + I_{K1} + I_{to} + I_{Kr} + I_{Ks} + I_{CaL} + I_{CaT} + I_{NaCa} + I_{NaK} + I_{pCa} + I_{pK} + I_{bCa} + I_{bNa} + I_f \quad (8)$$

Evaluating criterion of the pacemaking stability and ability

To analyse the effect of I_{K1} and I_f on pacemaking activity, we simulated the membrane potential under different current densities of I_{K1} and I_f with I_{K1} being reduced systematically by from between 60–100% (i.e., I_{K1} density at -80 mV changed from 0.396 to 0 pA/pF while the I_{K1} density in the original basal model is 0.99 pA/pF at -80 mV in I-V curve). The representative I-V relation curve under different inhibition of I_{K1} is shown in [S1A Fig](#). I_f density was increased by from 0 to 10 folds with a basal value of -0.63 pA/pF at -80 mV in I-V curve (i.e., I_f density changed from 0 to -6.3 pA/pF at -80 mV). The representative I-V relation curve under different incorporation of I_f is shown in [S1B Fig](#).

Two characteristics were used to quantify the state of membrane potentials generated by the ventricular pacemaker model: the continuity and validity of spontaneous APs. The continuity was used to quantify whether or not the automaticity of membrane potential could sustain with time; whilst the validity was used to characterize whether every automatic wave was biologically-valid or not. As such, we defined the following:

W: a valid wave. An action potential whose wave trough was less than -20 mV and wave crest was more than 20 mV could be considered as a valid wave.

αW , $\alpha < 1$: an incomplete wave.

R: a resting period lasting 1000 ms.

W^n : the concatenation of n W's.

(W R): the concatenation of W and R.

As such, the pacemaking behaviour of the I_{K1}/I_f pacemaker model can be categorized as FIVE states whose definitions were as followings:

None pacemaking behaviour during the entire simulation period could be described as State-1:

$$R^n, n \in N^+ \quad (9)$$

Transient spontaneous pacemaking behaviour could be described as State-2:

$$(W^m, R^n), m, n \in N^+ \quad (10)$$

Bursting pacemaking behaviour could be described as State-3:

$$(W^{m_i}, R^{n_i})^M, i \in [1, M], M, m_i, n_i \in N^+ \quad (11)$$

Persistent pacemaking activity with periodically incomplete depolarization could be described as State-4:

$$(W^m, \alpha W)^M, \alpha < 1, m, M \in N^+ \quad (12)$$

Stable pacemaking activity could be described as State-5:

$$W^m, m \in \mathbb{N}^+ \quad (13)$$

With regard to the pacemaking ability, when the pacemaking behaviour was stable, the cycle length (CL) under varied I_{K1} and I_f was calculated. The CL was defined as the averaged wavelength of pacemaking activity over a period of simulation of more than 400 s, ensuring the accuracy of the computed CL. As the basal model was for VMs, a long simulation period was necessitated to achieve a completely stable pacemaking status and minimize the effect of the transition period.

Characteristics of pacemaking during diastolic interval

The length of the diastolic interval (DI) is an important measure to characterize the pacemaking ability. In this study, we defined that DI as the time interval between the time of MDP (S2A Fig, t_1) and the time when the membrane potential reaches at -55 mV (i.e., around the activation potential of I_{CaL}) (S2A Fig, t_2). The diastolic upstroke velocity during DI was defined as the change rate of the membrane potential, taking the following formulation:

$$\text{diastolic upstroke velocity} = \frac{\text{MDP} - (-55)}{t_2 - t_1} \quad (14)$$

The unit of diastolic upstroke velocity was V/s.

We evaluated the contributions of all of the inward currents to membrane potential during DI and found that the main inward currents which helped to depolarize membrane potential during DI are I_{Na} , I_{NaCa} and I_f . Their contribution can be described by an average integral during DI:

$$I_{in} = \frac{\int_{t_1}^{t_2} (I_{Na} + I_{NaCa} + I_f)}{t_2 - t_1} \quad (15)$$

Similarly, the main outward currents which held membrane potential at diastolic potential during DI are I_{K1} , I_{NaK} , I_{Kr} and I_{Ks} , the integral of which can be described as:

$$I_{out} = \frac{\int_{t_1}^{t_2} (I_{K1} + I_{NaK} + I_{Kr} + I_{Ks})}{t_2 - t_1} \quad (16)$$

Results

Dynamic analysis in I_{K1}/I_f parameter space

Dynamic pacemaker AP behaviour was dependent on the balance of I_{K1} and I_f interactions. Simulations were conducted in the I_{K1}/I_f parameter space to characterize this dependence. Results are shown in Fig 1. With differing combinations of I_{K1} and I_f density, five different regions for distinctive pacemaking dynamics could be discerned, including stable pacemaking activity (blue area, State-5 defined by Eq 13), intermittence of failed depolarization (yellow area, State-4 defined by Eq 12), bursting pacemaking behaviour (orange area, State-3 defined by Eq 11), transient pacemaking activity (green area, State-2 defined by Eq 10), and no automaticity (grey area, State-1 defined by Eq 9). In each category, representative membrane potentials are illustrated at the bottom panel of Fig 1.

With a fixed I_f density, alterations to I_{K1} could produce different types of pacemaking activities, and this also applied when I_{K1} was fixed whilst I_f was changed. When I_f density was fixed at a density between -0.63 and -2.52 pA/pF, with a 60–80% block of I_{K1} (i.e., I_{K1} density at -80

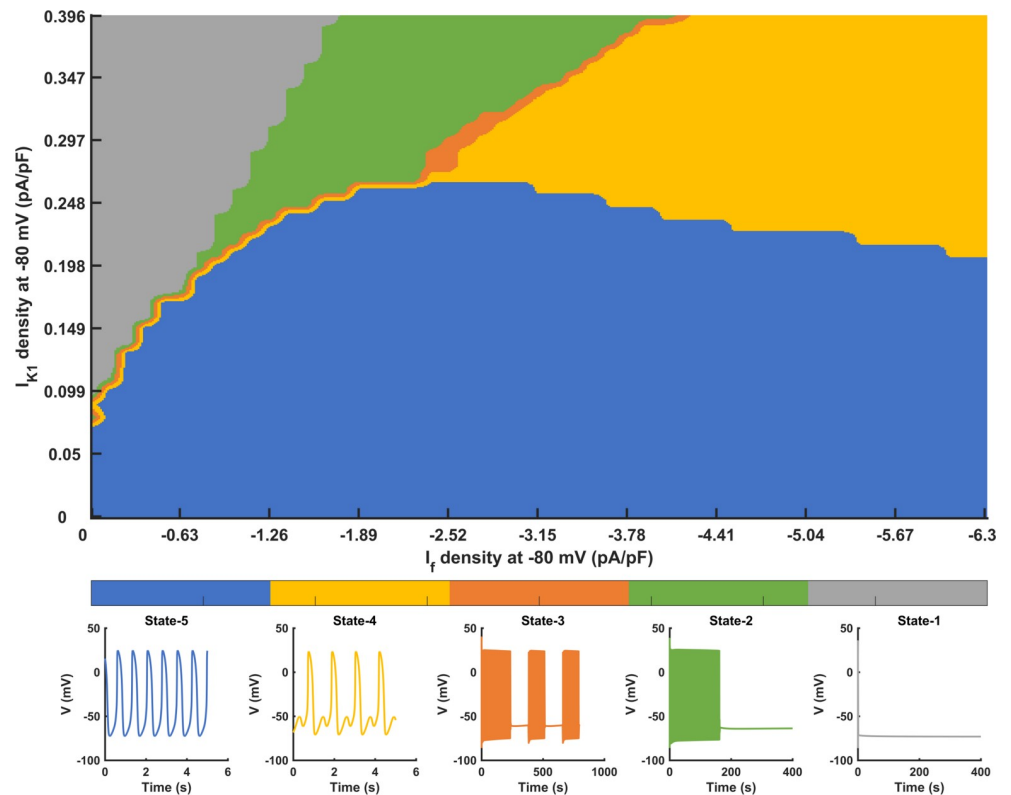


Fig 1. Dynamic behaviours of pacemaking action potentials in I_{K1}/I_f parameter space. Blue: stable pacemaking activity (State-5); Yellow: persistent pacemaking activity with periodic incomplete depolarization (State-4). Orange: bursting pacemaking behaviour (State-3). Green: transient spontaneous pacemaking behaviour (State-2). Gray: no spontaneous pacemaking behaviour (State-1). In each category, the typical pacemaking action potentials are illustrated at the bottom panel.

<https://doi.org/10.1371/journal.pcbi.1008177.g001>

mV was in the range of 0.198–0.396 pA/pF), pacemaking activity was generated but with self-termination (Fig 1, green area). Then, a further reduction in I_{K1} or a slight increase in I_f induced bursting pacemaking behaviour, as shown by the orange area in Fig 1, which was between the boundaries marking the persistent automaticity and transient pacemaking activity regions. A further increase in I_f or suppression in I_{K1} could produce persistent automaticity (Fig 1, yellow and blue area). But when I_{K1} was greater than about 0.248 pA/pF, incomplete depolarization appeared periodically (Fig 1, yellow area). Finally, a stable and spontaneous pacemaking activity could be generated when I_{K1} was decreased to less than 0.248 pA/pF at -80 mV with I_f included (Fig 1, blue area).

To illustrate possible reasons responsible for the effect of each changed ion current density on modulating pacemaking states, we chose four typical cases to analyze the corresponding pacemaking mechanisms in different pacemaking states in the I_{K1}/I_f parameter space. Cases are listed in Table 1.

Initiation of transient spontaneous depolarization

In the basal VM cell model with the suppression of I_{K1} by 70% (the density of I_{K1} at -80 mV was 0.297 pA/pF), incorporation of I_f (with a current density of -0.63 pA/pF) was unable to depolarize the membrane potential and lead to spontaneous pacemaking activity because the excessive outward current of I_{K1} counteracted the inward depolarizing current. This state can

Table 1. Typical cases and corresponding state.

CASE NO.	I_{K1} density (pA/pF)	I_f density (pA/pF)	State NO.
CASE 1	0.297 pA/pF	-1.89 pA/pF	State-2
CASE 2	0.297 pA/pF	-2.52 pA/pF	State-3
CASE 3	0.297 pA/pF	-3.15 pA/pF	State-4
CASE 4	0.248 pA/pF	-3.15 pA/pF	State-5

<https://doi.org/10.1371/journal.pcbi.1008177.t001>

be described by State-1 as shown in Eq 9. When the density of I_f was increased to -1.89 pA/pF, spontaneous depolarization was provoked at the beginning of the transition period, however, the automaticity self-terminated after 163 s (Fig 2A), showing a State-2 behaviour as described in Eq 10.

We analysed possible ion channel mechanisms responsible for unstable and self-terminating pacemaking APs with the current densities of (I_{K1} , I_f) at (0.297 pA/pF, -1.89 pA/pF) (defined as ‘CASE 1’). Results in Fig 2 showed that during the time course of the spontaneous pacemaking, there were changes of intracellular ionic concentrations and the MDP. There was an accumulation of the intracellular Ca^{2+} concentration ($[Ca^{2+}]_i$, Fig 2C) during the time course of spontaneous pacemaking APs. Such an accumulation of $[Ca^{2+}]_i$ was because the automaticity in VMs shortened the DI between two successive APs, leaving insufficient time for Ca^{2+} in the cytoplasm to be extruded to restore to its initial value after each cycle of excitation. This consequentially led to overload in $[Ca^{2+}]_i$, which suppressed the extent of the activation degree of the L-type calcium current (I_{CaL} , Fig 2F), especially during the phase 0 of the

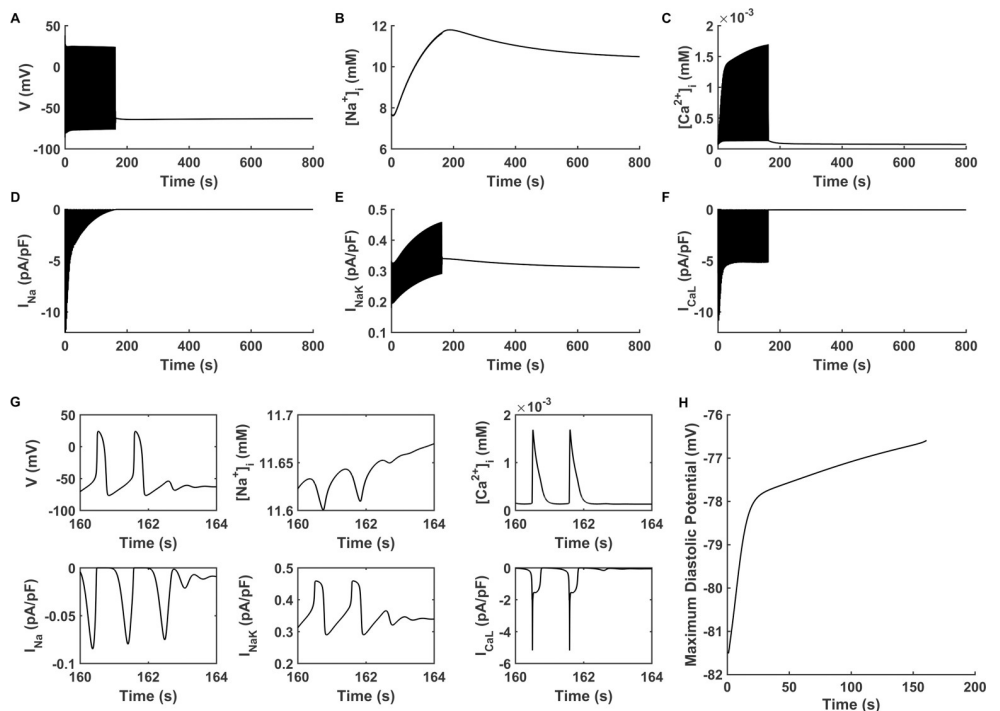


Fig 2. Transient spontaneous pacemaking behaviour. (A-F) Membrane potential (V), intracellular Na^+ concentration ($[Na^+]_i$), intracellular Ca^{2+} concentration ($[Ca^{2+}]_i$), fast sodium current (I_{Na}), Na^+/K^+ pumping current (I_{NaK}) and L-type calcium channel current (I_{CaL}) with the current densities of (I_{K1} , I_f) at (0.297 pA/pF, -1.89 pA/pF) (‘CASE 1’) during the entire simulating period of 800 s. (G) Expanded plots of (A-F) for the time course of pacemaking self-termination (160–164 s). H: Maximum diastolic potential of spontaneous pacemaking behaviour of (A).

<https://doi.org/10.1371/journal.pcbi.1008177.g002>

pacemaking action potential. Furthermore, the overloaded $[Ca^{2+}]_i$ increased the I_{NaCa} (S3A Fig) gradually with time, resulting in an elevated MDP (Fig 2H) that inhibited the activation degree of the fast sodium channel current (I_{Na} , Fig 2D). Through the Na^+ permeability of I_f , extra Na^+ flowed into the cytoplasm [53] during each of the APs. The increase of I_{NaCa} also accelerated the accumulation of the intracellular Na^+ concentration ($[Na^+]_i$) to increase from 7.67 to 11.8 mM (Fig 2B). The increased $[Na^+]_i$ augmented the feedback mechanism of Na^+/K^+ pumping activity, by which the Na^+/K^+ pump current (I_{NaK}) increased gradually with time (Fig 2E). All of these factors worked together, inhibiting the membrane potential to reach the take-off potential, leading to self-terminated automaticity at 163 s (Fig 2G).

It was also possible to generate automaticity in the model by fixing the current density of I_f at a low value, but with a further reduction in I_{K1} density. S4 Fig shows the results when I_f was held at -0.63 pA/pF and the current density of I_{K1} was reduced to 0.178 pA/pF. In this case, pacemaking activity appeared in the model, but the automaticity was unstable and self-terminated due to similar mechanisms as shown in Fig 2 for the increased- I_f situation.

Bursting pacemaking behaviour

Fig 3 shows the intermittent bursting behaviour, which is generated with a different combination of I_{K1} and I_f current densities in the model. In the figure, the current densities of (I_{K1} , I_f) were at (0.297 pA/pF, -2.52 pA/pF) (defined as ‘CASE 2’). Such kind of pacemaking state can be classified as State-3 (Eq 11).

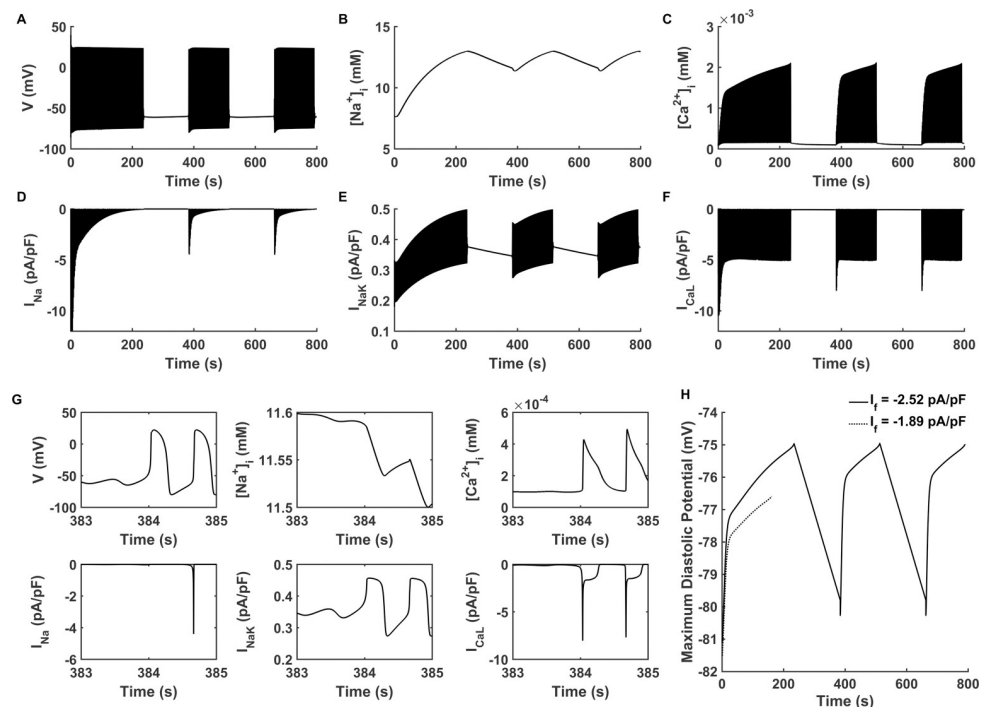


Fig 3. Bursting pacemaking behaviour. (A-F) Membrane potential (V), intracellular Na^+ concentration ($[Na^+]_i$), intracellular Ca^{2+} concentration ($[Ca^{2+}]_i$), fast sodium channel current (I_{Na}), Na^+/K^+ pumping current (I_{NaK}) and L-type calcium channel current (I_{CaL}) with the current densities of (I_{K1} , I_f) at (0.297 pA/pF, -2.52 pA/pF) (‘CASE 2’) during the entire simulating period of 800 s. (G) Expanded plots of (A-F) for the time course of pacemaking resumption (383–385 s). (H) Maximum diastolic potential of automatic pacemaking activity when I_f is -2.52 and -1.89 pA/pF (‘CASE 2’ vs. ‘CASE 1’, solid and dotted line respectively).

<https://doi.org/10.1371/journal.pcbi.1008177.g003>

In ‘CASE 2’, the spontaneous oscillation was unstable, characterized by self-termination and then resumption after a quiescent period (Fig 3A). During the first pacemaking stage (simulation period from 0 to 236 s in Fig 3), the self-termination was accompanied by the overload of $[Na^+]_i$, the accumulation of $[Ca^{2+}]_i$, which caused the reduction of I_{Na} , the increase of I_{NaK} and the decrease of I_{CaL} (Fig 3B–3F). An increased $[Na^+]_i$, accumulated $[Ca^{2+}]_i$, reduced I_{Na} , increased I_{NaK} and decreased I_{CaL} can also be observed in the pacemaking stage in Fig 2. This suggested that the underlying mechanisms responsible for the self-termination of the pacemaking APs were similar to those of ‘CASE 1’.

It is of interest to analyse the mechanism(s) for the resumption of the pacemaking APs after a long pause. It was shown that, during the time course of the quiescent interval (236–384 s in Fig 3A–3F), the intracellular Na^+ (Fig 3B) continued to be extruded out of the cell by I_{NaK} (Fig 3E). As such, the $[Na^+]_i$ (Fig 3B) gradually decreased over time. The decrease in $[Na^+]_i$ led to a gradually reduced I_{NaK} over the time course of quiescence (Fig 3E), which decreased the suppressive effect of I_{NaK} on depolarization. Via I_{NaCa} (S3B Fig), the intracellular Ca^{2+} was kept to be extruded out of the cell, leading to a decreased $[Ca^{2+}]_i$ (Fig 3C). The reduction in $[Ca^{2+}]_i$ reduced the Ca-induced inactivation gate of I_{CaL} , resulting in an increased I_{CaL} . Ca^{2+} concentration in the sarcoplasmic reticulum ($[Ca^{2+}]_{SR}$) also decreased via a leakage Ca release (I_{leak}) from SR to cytoplasm (S8C–S8D Fig) because of the reduced $[Ca^{2+}]_i$. Moreover, as compared with ‘CASE 1’, the increase in I_f helped to produce a more depolarized MDP (Fig 3H), allowing the membrane potential more easily to reach the take-off potential for initiation of the upstroke. During the quiescent stage, I_{CaL} and I_{Na} kept at a small magnitude (Fig 3D and 3F) because of the quiescent membrane potential at which little I_{CaL} and I_{Na} were activated. Until the Ca^{2+} oscillation produced a full course of action potential with a sufficiently depolarised MDP, I_f and I_{Na} was fully activated, facilitating the resumption of the spontaneous pacemaking activity at 385 s (Fig 3G). This process of self-termination and resumption repeated alternately, which constituted bursting behaviour.

Persistent pacemaking activity

A further increase in I_f ((I_{K1}, I_f) at (0.297 pA/pF, -3.15 pA/pF)) produced a series of persistent spontaneous APs. Results are shown in Fig 4 (grey lines) for APs (Fig 4A), together with a phase portrait of membrane potential (V) and total membrane channel current (I_{total}) (Fig 4B), I_{K1} (Fig 4C), and I_{CaL} (Fig 4D). Although the spontaneous APs were sustained during the entire simulation period of 800 s, there were some incomplete depolarizations observed periodically (Fig 4A, grey line) which can be classified as State-4 according to Eq 12. This pacemaking situation was termed as ‘CASE 3’.

When the density of I_{K1} was further reduced to 0.248 pA/pF (Fig 4C, black line), a stable pacemaking activity was established (Fig 4A, black line), with an average CL of 895 ms and MDP of -72.63 mV. This kind of pacemaking state can be described as State-5 by Eq 13. In this condition, the pacemaking activity was robust and the pacing CL was close to that of the native human SAN cells (approximately 800–1000 ms [55]). We termed stable pacemaking activity with (I_{K1}, I_f) at (0.248 pA/pF, -3.15 pA/pF) as ‘CASE 4’.

In order to understand potential mechanism(s) underlying the genesis of incomplete pacemaking potentials in CASE 3, phase portraits of membrane potential against I_{total} for incomplete (grey line) and complete (black line) depolarization APs were plotted and superimposed for comparison, as shown in Fig 4B, with a highlight of phase portraits during the diastolic pacemaking potential range from -75 mV to about -45 mV being shown in the inset. In the case of incomplete depolarization (CASE 3), there was a greater I_{K1} (Fig 4C) that counteracted the inward depolarizing current, leading to a smaller I_{total} during the diastolic depolarization

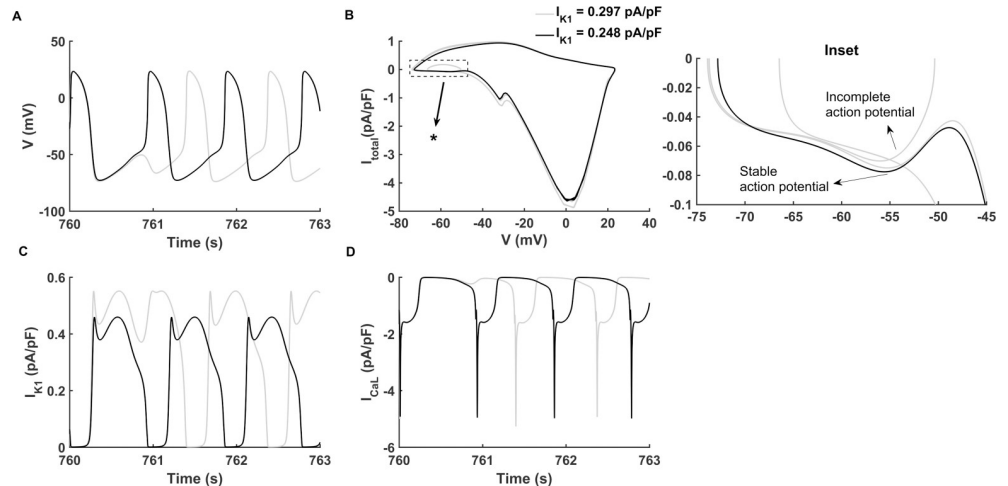


Fig 4. Persistent pacemaking activity. The current densities of (I_{K1} , I_f) of stable pacemaking activity and periodically incomplete pacemaking activity are at (0.248 pA/pF, -3.15 pA/pF) ('CASE 4', black lines) and (0.297 pA/pF, -3.15 pA/pF) ('CASE 3', grey lines) respectively. (A-D) The membrane potential (V), phase portraits of membrane potential against the total membrane channel current (I_{total}), inward rectifier potassium channel current (I_{K1}) and L-type calcium channel current (I_{CaL}) during the simulating time course of 760–763 s. (Inset) Expanded plot during V from -75 to -45 mV and I_{total} from -0.1 to 0 pA/pF marked by the asterisk in (B).

<https://doi.org/10.1371/journal.pcbi.1008177.g004>

phase (see the grey line in Fig 4B and the inset). Consequentially the membrane potential failed to reach the take-off potential for the activation of I_{CaL} (Fig 4D, grey line), leading to an incomplete course of action potential (Fig 4A, grey line). In CASE 4, with a reduced I_{K1} (Fig 4C, black line), there was a greater I_{total} during the diastolic depolarization phase (Fig 4B and the inset, black line), which drove the membrane potential to reach the take-off potential for the activation of I_{CaL} (Fig 4D, black line), leading to the upstroke of the action potential.

The frequency for the appearance of the incomplete AP was dependent on the density of I_{K1} . Incomplete depolarization occurred less frequently, with progressively smaller I_{K1} . By way of illustration, the incomplete depolarization appeared once every three cycles with the I_{K1} density at 0.297 pA/pF in CASE 3 (S5A Fig), but this became once every five cycles when I_{K1} density was reduced to 0.277 pA/pF I_{K1} (S5B Fig). This suggested that a large residual of I_{K1} in the VM model might result in the failure of complete depolarization.

Pacemaking cycle length in I_{K1}/I_f parameter space

A systematic analysis of the relationship between the calculated CL in the I_{K1} and I_f density parameter space is presented in Fig 5. In the figure, the measured CL was coloured from 650 ms in dark red to 1000 ms in yellow. In this study, we regarded persistent pacemaking action potential with CL 1000 ms or less as 'valid pacemaking activity' (corresponding to 'State-5' with CL \leq 1000 ms in Fig 1), therefore, only the CLs of the valid pacemaking potentials are shown in Fig 5.

It was shown that a sufficient depression in I_{K1} (up to 75%; I_{K1} density $<$ 0.248 pA/pF) was required to produce a stable pacemaking action potential with a 'valid' pacemaking frequency. With the increase of the I_{K1} inhibition level, the CL became shortened at all I_f densities considered. Also, the more that I_{K1} was inhibited, the less I_f was needed to provoke 'valid' spontaneous pacemaking activity. By contrast, the effect of I_f on the CL presented two phases, which was dependent on the I_{K1} density. When I_{K1} was less than 0.198 pA/pF, the pacemaking ability became robust with the increase in I_f density. However, when I_{K1} was increased from 0.198 to

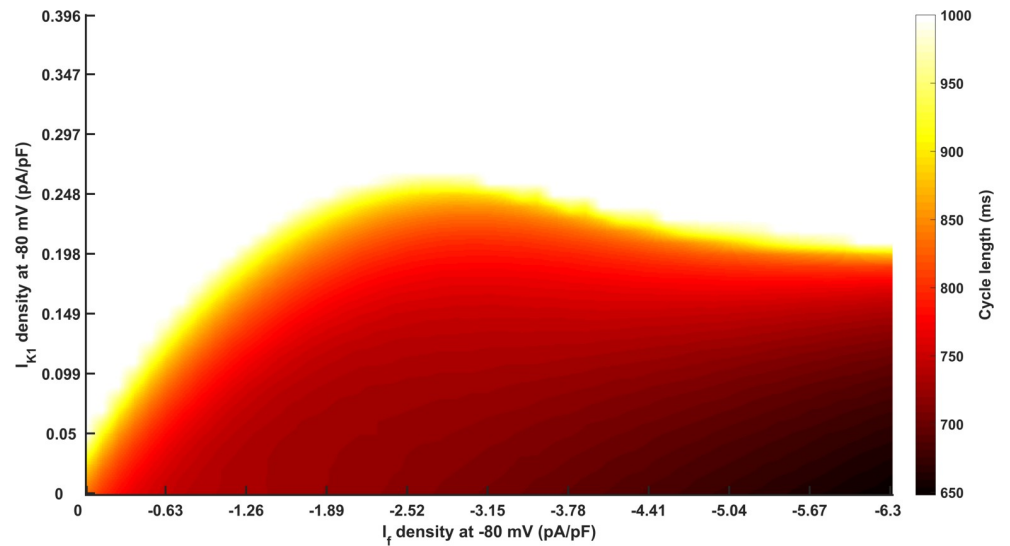


Fig 5. Measured cycle length in I_{K1}/I_f parameter space. The density of I_{K1} is from 0 to 0.396 pA/pF and the density of I_f is from 0 to -6.3 pA/pF at -80 mV. The measured cycle length (CL) is coloured from 650 ms in dark red to 1000 ms in yellow. White means that there is no definitely measured pacemaking CL (i.e., the pacemaking action potential is not persistent or stable) or the pacemaking activity is 'invalid' (CL > 1000 ms).

<https://doi.org/10.1371/journal.pcbi.1008177.g005>

0.248 pA/pF, an increase in I_f actually slowed the pacemaking activity, leading to an increased CL.

Reciprocal role of I_f and I_{K1} in generating pacemaking APs

Further analysis was conducted to investigate the reciprocal role of reduced I_{K1} and increased I_f in generating pacemaking APs. This section analysed the role of I_f and I_{K1} in the parameter space which produced stable pacemaking activity (the 'State-5' in Fig 1) with the density of I_{K1} at 0.05 and 0.198 pA/pF. By sufficiently reducing I_{K1} to a density of 0.05 pA/pF alone (in the absence of I_f), the model was able to generate stable spontaneous APs with a CL of 1011 ms (S6A and S6E Fig, dotted lines). In this case, the incorporation of I_f with a small density helped to boost the pacemaking activity and increase the pacemaking frequency. It was shown that with the incorporation of I_f at a density of -0.63 pA/pF, the CL was reduced by 233 ms, changing from 1011 ms to 778 ms (S6A Fig). Compared with the case of I_f absence, incorporation of I_f —even with a small density—helped to depolarize cell membrane potential during the early DI phase (S6A and S6C Fig). Moreover, a similar phenomenon to Fig 2 was that the incorporation of I_f led to an accumulation of $[Na^+]_i$ (S6B Fig) and $[Ca^{2+}]_i$ (S6D Fig and Inset C). The accumulation of $[Ca^{2+}]_i$ increased I_{NaCa} (S6F Fig) which contributed to the depolarization of membrane potential. As a result, the incorporation of I_f facilitated genesis of spontaneous APs and shortened the DI significantly thus decreased the CL.

With a fixed I_{K1} density of 0.05 pA/pF, the relationship between the computed CL of pacemaking APs and I_f density was shown in Fig 6A. In a range from 0 to -2.52 pA/pF, an increase in I_f density produced a marked decrease in the CL (Fig 6A), which was associated with an increase in the rate of membrane depolarization during the DI (diastolic depolarizing rate) (S2B Fig). In this range, an increase in I_f caused an accumulation of $[Na^+]_i$ (Fig 6C), which enhanced I_{NaCa} (Fig 6D). Particularly, there was a precipitous decline of I_{Na} when I_f was in the range from 0 to -1.26 pA/pF (Fig 6F). This was because the augmented I_f elevated the MDP of the action potential (Fig 6B), which affected the activation level of I_{Na} . Furthermore, when I_f

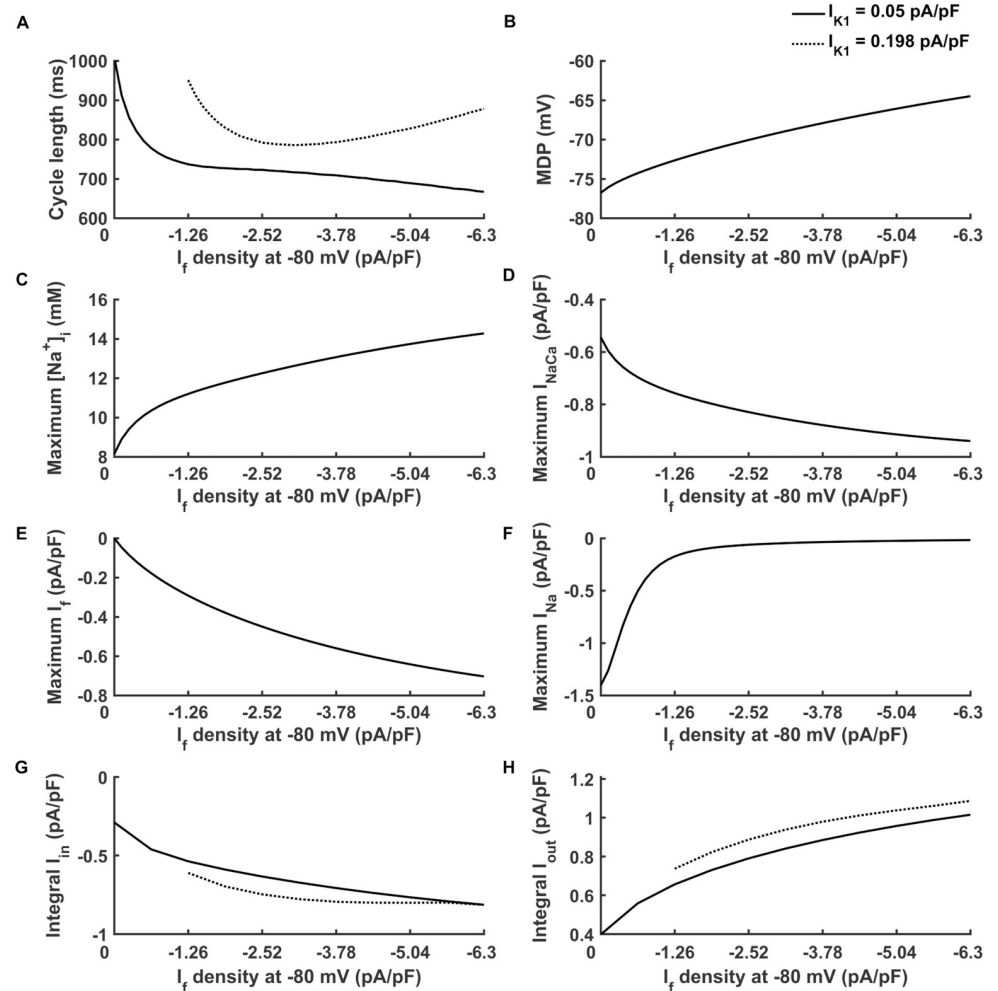


Fig 6. Effect of I_f density on the pacemaking cycle length under different I_{K1} density. (A) Change of cycle length with the increase of I_f from 0 to -6.3 pA/pF when I_{K1} density is 0.05 (solid line) and 0.198 pA/pF (dotted line). (B-F) Change of maximum diastolic potential (MDP), maximum intracellular Na^+ concentration ($[\text{Na}^+]_i$), maximum Na^+ / Ca^{2+} exchange current (I_{NaCa}), maximum funny current (I_f) and maximum fast sodium current (I_{Na}) during a pacemaking period with the increase of I_f from 0 to -6.3 pA/pF. (G-H) Change of the normalized total integral of main inward currents (Integral I_{in}) and normalized total integral of main outward currents (Integral I_{out}) during DI phase with the increase of I_f when I_{K1} density is 0.05 (solid line) and 0.198 pA/pF (dotted line). The inward currents include I_{Na} , I_{NaCa} and I_f ; the outward currents include inward rectifier potassium channel current (I_{K1}), Na^+/K^+ pumping current (I_{NaK}), rapid delayed rectifier potassium channel current (I_{Kr}) and slow delayed rectifier potassium channel current (I_{Ks}).

<https://doi.org/10.1371/journal.pcbi.1008177.g006>

density was over -2.52 pA/pF, there was a less dramatic decrease in CL with an increase of I_f (Fig 6A). This was attributable to a reduced I_{Na} (Fig 6F) as a consequence of the gradual elevation of the MDP (Fig 6B). Another factor was that the maximum density of I_f was not increased linearly (Fig 6E) because of elevated MDP.

Depending on the I_{K1} density, the relationship between CL and I_f density could also be bi-phasic. With a small I_{K1} density (0.05 pA/pF), the measured CL decreased monotonically with the increase in I_f density (Fig 6A, solid line). However, with a large I_{K1} (0.198 pA/pF), the measured CL first decreased with an increased I_f density, but then increased with it when I_f density was greater than -3.15 pA/pF, implicating a slowdown in the pacemaking activity with the increase of I_f (Fig 6A, dotted line). The action potentials with the current densities of (I_{K1} , I_f) at

(0.198 pA/pF, -3.78 pA/pF) and (0.198 pA/pF, -5.04 pA/pF) indicated that such a slowdown of pacemaking APs with an increased I_f was mainly due to the prolonged DI (S1 Text). The extra I_f accelerated pacemaking activity, leaving insufficient time for intracellular Ca^{2+} to be extruded, which resulted in a higher amplitude of $[Ca^{2+}]_i$ (Fig A in S1 Text). As a consequence, I_{NaCa} amplitude increased, leading to an increased $[Na^+]_i$, and finally an increased outward I_{NaK} (Fig B in S1 Text). At the same time, I_f elevated the MDP (Table A in S1 Text), so the amplitude of I_{Na} decreased (Fig B in S1 Text). The changes in these currents caused a prolonged CL at a great I_f density. This indicated that the bi-phasic effect of I_f may be attributable to the delicate balance between inward currents and outward currents during the DI phase. To extend this hypothesis to the whole I_f parameter space, I_{in} and I_{out} were defined as the total integral of three dominant inward currents during the DI phase (I_{Na} , I_{NaCa} and I_f) (Eq 15) and the total integral of four dominant outward currents during the DI phase (I_{K1} , I_{NaK} , I_{Kr} and I_{Ks}) (Eq 16). At a low I_{K1} density of 0.05 pA/pF, with the increase in I_f density, there was a monotonic decrease of CL (Fig 6A, solid line). However, at a large I_{K1} density (e.g., 0.198 pA/pF), more than -3.15 pA/pF I_f resulted in an increased CL (Fig 6A, dotted line). This observation can be explained by the unsaturated I_{in} . The density of I_{in} was an integrated consequence of MDP, the activation degree of I_{Na} and I_f , as well as the density of I_{NaCa} . At 0.05 pA/pF I_{K1} density, I_{out} was small, therefore I_{Na} , I_{NaCa} and I_f was saturated (i.e., I_{in} was saturated). However, when I_{K1} was large, increased I_{out} led to a more negative MDP which resulted in an increased I_{in} due to more activated I_{Na} , I_{NaCa} and I_f . But I_{in} reached at a asymptotic value after I_f density was greater than -3.15 pA/pF (Fig 6G, dotted line) because the a similar level of the diastolic $[Ca^{2+}]_i$ (i.e., minimum $[Ca^{2+}]_i$) at different I_{K1} caused a decreased normalized integral of I_{NaCa} (Fig C in S1 Text), therefore I_{in} was not saturated at large I_{K1} (Fig 6G, dotted line). Consequentially, the I_{out} outbalanced the I_{in} , leading to a prolonged DI that increased the CL at large I_{K1} .

Incorporation of I_{CaT} in I_{K1}/I_f pacemaker model

The incorporation of I_{CaT} in the I_{K1}/I_f pacemaker model with the current densities of (I_{K1} , I_f) at (0.297 pA/pF, -0.63 pA/pF) induced automaticity in non-pacemaking cell model (S7A Fig). It was shown that I_{CaT} initiated the oscillation of Ca^{2+} in the cytoplasm and the SR (S7B and S7C Fig) in the non-pacemaking cell model, activating the I_{NaCa} and I_{CaL} (S7D and S7E Fig).

However, when I_{CaT} was incorporated into a stable I_{K1}/I_f pacemaker model with the current densities of (I_{K1} , I_f) at (0.099 pA/pF, -0.63 pA/pF), an increased pacemaking CL was observed (853 ms vs. 950 ms, S8A Fig). The reason was that the addition of I_{CaT} in the model affected the Ca^{2+} dynamics, resulting in an accumulation of $[Ca^{2+}]_i$ as well as $[Ca^{2+}]_{SR}$, leading to an increased I_{NaCa} and greater inactivation of I_{CaL} (S8C–S8F Fig). An increased I_{NaCa} consequently caused an accumulation of $[Na^+]_i$, leading to an increased outward I_{NaK} (S8G Fig). More importantly, an increased I_{NaCa} elevated the MDP, leading to a less activated I_{Na} and I_f (S8H and S8I Fig). These together with an increased I_{NaK} produced a prolonged CL.

Discussion

Summary of major findings

Biological experiments provided possibilities to transform non-pacemaking CMs or stem cells into bio-pacemaker cells by regulating the expression of I_f [13,28,29,36,37] or I_{K1} [11,20,21]. Computationally, bifurcation theory was used to analyse the effect of the density of an individual ion channel current on the membrane potential of a cardiac cell [47,50], by which decisive currents in pacemaking initiation can be screened out. The interaction between multiple ion channels in cardiac pacemaking has also been considered in some prior studies. Lakatta et al.

[51] investigated the effect of multiple component ion channels on cardiac pacemaking by identifying numerically minimal ensembles of ion channels in the SAN model. Their study provided a simplification of the model which may be suitable for further bifurcation analysis. However, due to the simplification, the model does not reflect the whole ionic dynamics of cardiac cells. In another study, Kurata et al. [50] simulated the combined action of I_f and I_{CaT} , I_{st} or I_{CaL} with three specific values of I_{CaT} , I_{st} or I_{CaL} considered. That study also suggested that there was a threshold of I_{K1} below which automaticity can be induced in I_f -incorporated ventricular model, but potential underlying ionic mechanisms on how balanced I_{K1}/I_f modulates the stability of the pacemaking activity was not shown. Considering the biological possibility that the superiority of combined action of I_{K1} and I_f [10,32,44] and unclear interaction between I_{K1} and I_f in the initiation of stable pacemaking activity in a whole cardiac cell model, the present study developed a virtual bio-engineered pacemaking cell model based on a human ventricular model by downregulating of I_{K1} and incorporating I_f . In comparison with previous computational modelling studies on bio-pacemakers [50,51], the present study provides new insights into understandings of 1) the dynamic regulation of ionic concentrations and ionic channel currents in I_{K1}/I_f -induced ventricular pacemaker; 2) the interaction between I_{K1} and I_f in the genesis of pacemaking action potentials; and 3) the stability of pacemaking potentials in wide I_{K1}/I_f parameter space.

The present I_{K1}/I_f pacemaker model can initiate robust and stable pacemaking activity by balancing the actions of reduced I_{K1} and increased I_f , though the effect of each manipulation on pacemaking activity is different. While the action of a reduced I_{K1} on the pacemaking activity is monophasic, that of an increased I_f is biphasic. It was shown that inhibiting I_{K1} promotes pacemaking ability and stability. The incorporation of I_f at an appropriate level promotes pacemaking activity, but an excessive I_f might result in abnormal pacemaking activity accompanied by abnormal intracellular ionic concentrations (such as pacemaking activity with periodically incomplete depolarization) or weak pacemaking ability, which could be proarrhythmic. As a result, the reciprocal interaction between I_{K1} and I_f is crucial for producing stable spontaneous pacemaking activity in VMs. In the present model, specific I_f density at different I_{K1} densities or vice versa was suggested.

This study demonstrated the feasibility of creating VM-based pacemaker cells by downregulating I_{K1} and upregulating I_f and provided evidence of the superiority of I_{K1}/I_f -based pacemaker model theoretically. The results of this study may be useful for optimizing the future design of engineered bio-pacemakers.

Role of I_{K1} suppression on pacemaking activity

Simulation results that suppressing I_{K1} by 75% - 100% can initiate stable pacemaking behaviour are in consistence with those of experimental findings, where it has been found that more than 80% inhibition of I_{K1} was required to produce a pacemaking phenomenon in guinea-pig's ventricular cavity [11,21]. It is also in agreement with previous bifurcation analyses in showing that it required I_{K1} to be reduced to at least 15% of the control value to transform a VM cell model to be auto-rhythmic [47]. And a complete block of I_{K1} produced a spontaneous pacemaking activity with a CL of 795 ms [47], close to 833 ms when I_{K1} was completely suppressed in the present study. The effect of I_{K1} suppression on pacemaking activity was monotonic in our pacemaker model. The more the I_{K1} is blocked, the faster the pacemaking activity is with all I_f densities considered. Similar results have also been observed in another human ventricular cell model [56] based on modifications of the O'Hara and Rudy model (ORD model) [57] (Fig A in S2 Text, solid and dotted lines).

Though our simulation results suggest an important role of sufficient suppression of I_{K1} in generating persistent and stable pacemaking APs, it is noteworthy that the deficiency of I_{K1}

has been reported to be lethal for adult rodents [58]; and loss function of *Kir2* gene may prolong QT intervals as well as cause Andersen's syndrome [59]. Consequently, suppression of I_{K1} from VM for generating a biological pacemaker may only be suitable when applied to highly localized, designated 'pacemaker' regions.

Role of I_f on pacemaking activity

I_f has been shown to play an important role in generating pacemaking APs in both native [13,22,28,29,36,37] and engineered pacemakers [43]. Experimentally it has been shown that high expression of *HCN2* can initiate spontaneous beats in neonatal rat VMs [22,36] and improve spontaneous beats in rabbit CMs [13]. *HCN4* incorporation by the expression of *TBX18* can also initiate spontaneous pacemaking activity in both rodent VMs [10] and porcine VMs [12].

In the present study, I_f helped to promote pacemaking activity, *via* its action of depolarization during the diastolic depolarization phase as well as its action on the intracellular ion concentrations. The inclusion of I_f in the VM cell model caused the accumulation of $[Na^+]_i$ by Na^+ channel of I_f [53]. The enhanced pacemaking activity caused by extra I_f also induced the accumulation $[Ca^{2+}]_i$ because there was not enough time to extrude Ca^{2+} from the cytoplasm [60]. The accumulated $[Ca^{2+}]_i$ increased I_{NaCa} , which promoted membrane potential depolarization especially during the early stage of DI (S6 Fig). Such a promoting action of I_f in bio-pacemaking can also be seen in another independent model as shown in S2 Text.

The increase in I_f density can enhance the automaticity in most cases. However, the effect of I_f on the pacemaking activity was observed to be bi-phasic. When it was increased to be over a threshold, excessive I_f resulted in an elevated MDP (Fig 6), which caused a reduced activation of I_f and I_{Na} , leading to a slowdown of the ability of pacemaking activity. This phenomenon occurred when the I_{K1} was not suppressed sufficiently. The impairing effect of excessive I_f on pacemaking APs was also observed in another ventricular pacemaker model based on modification of the ORD model [56] (S2 Text). It was shown that a greater increase in I_f density even terminated pacemaking activity (Fig B in S2 Text). The possible impairing effect of I_f on I_{Na} was verified by the fact that in the bio-pacemaker induced by *HCN2* expression [61], co-expression of the skeletal muscle sodium channel 1 (*SkM1*), in order to hyperpolarize the action potential threshold, helped to counterbalance the negative effect of I_f overexpression, producing an accelerated depolarization phase. In fact, in the original TP06 model, the peak amplitude of I_{Na} was about -300 pA/pF at the resting potential of -86.2 mV [54]. In our pacemaker model, the peak amplitude of I_{Na} was significantly reduced because of the elevated MDP. This suggested that to counterbalance the elevated MDP and the reduced I_{Na} , an increase in the channel expression of I_{Na} may help to produce an enhanced pacemaker. This might be simulated by increasing I_{Na} conductance in the model study. Furthermore, when I_{K1} was large, an increase in I_f even lengthened pacemaking period or caused unstable pacemaking behaviour (Fig 1). This simulation result is in agreement with a previous biological experimental study that observed arrhythmicity when acute *HCN* gene was expressed [42]. Another experimental study showed that *HCN2*-expression caused an excessive increase in the basal beating rate [62]. In our model, it has been also observed that excessive I_f may cause an overly fast pacemaking rate.

Reciprocal interaction between I_{K1} and I_f

Our study demonstrates that the reciprocal interaction between I_{K1} and I_f plays a crucial role in creating stable and persistent pacemaking. Only an optimal combination of I_{K1} and I_f can initiate stable pacemaking activity. In the present pacemaker model, the greater the degree of

I_{K1} suppression, the smaller was the I_f density required for the generation of spontaneous oscillation (Fig 1). And modulation of the two currents simultaneously helps to create a physiologically-like pacemaker that is better than that produced by manipulating I_{K1} or I_f alone (Fig 5). Such observation of reciprocal interaction between I_{K1} and I_f in pacemaking is consistent with previous experimental observations. Previous studies have shown that although suppressing I_{K1} [11,21], or incorporating sufficient I_f [22] alone was able to initiate pacemaking activity in VM cells, a pacemaker constructed by *TBX18* showed greater stability, due to its combined actions of I_{K1} reduction and I_f increase [10]. Another experiment in porcine VMs [12] also indicated that *TBX18* expression did not increase the risk of arrhythmia, which means that a mixed-current approach is probably a superior means of producing a bio-pacemaker. Experiments in a *Kir2.1/HCN2* HEK293 cell [45] and *Kir2.1/HCN4* [43] showed that I_{K1} may actually recruit more I_f by activating current at more negative membrane voltages because I_{K1} was the only hyperpolarizing current in these experiments. Our simulations, however, did not yield such a result because the interaction of other outward currents (such as I_{NaK} , I_{Kr} and I_{Ks}) contributed to the hyperpolarization of membrane potential and helped the activation of I_f . We thought an integrated action between all of ionic currents in cardiac cells should be considered, rather than evaluated specific ionic currents in a partial model.

In addition, simulation results indicated that I_{K1} expression level may influence the I_f 's effect on the pacemaking activity (Fig 6A). Excessive I_{K1} hindered I_f 's ability to modulate pacemaking activity. This further showed that the balanced expression of I_{K1} and I_f affected the balance between the inward and outward currents during the diastolic depolarization phase, thus affected the membrane potential state and the pacemaking CL of the pacemaker. An experiment showed a coincident result that the expression of *HCN2* in adult rat VMs could not cause spontaneous beats due to the high expression of I_{K1} [22], but in neonatal rats, the I_{K1} was less so that expressing *HCN2* could provoke automaticity. Similarly, such a dynamic balance between the inward and outward currents during the repolarization and the diastolic depolarization phase was also affected by other repolarization currents, such as I_{Kr} , I_{Ks} and I_{NaK} etc. Possible effects of modulating these repolarization currents on the bio-pacemaking warrants further studies in the future.

The present I_{K1}/I_f -induced pacemaker model exhibited greater robustness than I_{K1} -based or I_f -based pacemaker models. In the I_{K1} -based model, the range of I_{K1} density that could initiate spontaneous beatings was from 0 to 0.0246 pA/pF, while in I_{K1}/I_f -based pacemaker model, this value extended to 0.248 pA/pF (Fig 1). The superiority of I_{K1}/I_f -based pacemaker model than I_f -based pacemaker model seemed to be more distinct. Incorporating I_f alone at a high density of -6.3 pA/pF could not provoke any spontaneous beating, but combining with the suppression of I_{K1} , small incorporation of I_f helped to ignite automaticity (Fig 1). The flexibility of this system also reflected in the easy modulation of CL *via* manipulating I_{K1} and I_f density (Fig 5).

Compared with the human SAN cell model developed by Fabbri et al. [53] and human SAN cell [64], the action potential generated by the I_{K1}/I_f -induced pacemaker model had a longer action potential duration at 90% (APD90) and a more negative MDP when the CL was similar (see Table 2). Such differences may be attributable to the fact that there are regional differences in the functional expression of ionic currents between the SAN and ventricular myocytes [63]. In the presented I_{K1}/I_f -induced pacemaker model, though we have reduced I_{K1} and incorporated I_f to a similar level of ion channel current densities as the SAN, other ionic currents in the present I_{K1}/I_f -induced pacemaker model inherited the same channel properties of VMs cell model, causing different pacemaker behaviour in the I_{K1}/I_f biological pacemaker model as compared to the SAN model.

Table 2. Comparison of pacemaker behaviours between the SAN cell and the bio-pacemaker cell.

Type	CL (ms)	APD90 (ms)	MDP (mV)
Human SAN Experiment [64]	828 ± 21	143.5 ± 49.3	-61.7 ± 6.1
Human SAN Model [53]	814	161.5	-58.9
Human Bio-pacemaker Model*	817	299	-75.1683

* The current densities of (I_{K1} , I_f) is (0.1 pA/pF, -0.882 pA/pF).

<https://doi.org/10.1371/journal.pcbi.1008177.t002>

Ca²⁺ dynamics in I_{K1}/I_f pacemaker model

There is still debate about the relative role of two pacemaking mechanisms of membrane clock (I_f) and Ca²⁺ clock [65]. A biological experiment demonstrated that Ca²⁺-stimulated adenylyl cyclase AC1 can promote pacemaking ability in *HCN2*-expressed left bundle branches [62]. A model study [66] that evaluated the synergism between Ca²⁺ clock and membrane clock in SAN central cell, also showed that the synergistic system was more robust and flexible. Another study [67] showed that VMs may also have Ca²⁺ clock, which provided a probability for the creation of Ca²⁺ clock-based bio-pacemaker. The role of Ca²⁺ dynamics in bio-pacemaker was also shown in our I_{K1}/I_f pacemaker model. As shown in Fig 3G, the resumption of pacemaking activity in bursting behaviour was provoked by the oscillation of $[Ca^{2+}]_i$. This indicated that the Ca²⁺ dynamics played an important role in the creation of bio-pacemaker, which warrants further study.

Furthermore, considering the role of I_{CaT} in the genesis of pacemaking APs in native SAN cells, a theoretical investigation of potential role(s) of I_{CaT} in the bio-pacemaker was conducted using the I_{K1}/I_f -modulated pacemaker model. It was shown the effect of I_{CaT} had dual aspects. On one hand, the incorporation of I_{CaT} might promote the pacemaking ability of ventricular pacemaker [50], by initiating Ca²⁺ oscillation thus producing spontaneous beatings in quiet pacemaker model. On the other hand, the incorporation of I_{CaT} might affect the MDP, leading to secondary actions on the homeostasis of ion concentrations, as well as ion channel currents including I_{Na} , I_b , I_{NaCa} and I_{NaK} , which slowed down the pacemaking activity.

Limitations

Limitations of the human VMs model we used in this study has been described elsewhere [54]. In this study, the I_f formulation of human SAN [53] was incorporated into the original VMs model. The properties of I_b , including the conductance of I_b , the half-maximal activation voltage ($V_{1/2}$) and time constants of the activation, may present species-dependence. In the present version, we only consider the conductance of I_f but have not discussed other properties of I_f . Moreover, in this study, we only investigated the pacemaking action potential at the single-cell level, without considering the intercellular electrical coupling between pacemaker cells as presented in the SAN tissue. These limitations are now being addressed for future versions of the model. In addition, bio-pacemaker models developed from other cardiac cell types, such as atrial myocytes, warrant future studies. Additionally, the other pacemaking-related currents in native SAN cells, such as I_{Na} and I_{sb} , could also be adjusted for creating stable bio-pacemaker.

One of possible advantages of bio-pacemaker over the traditional electronic pacemaker is at its possible sensitivity to autonomic regulation. It is of interest to study how the pacemaking action potentials are modulated by autonomic regulation by β -Adrenergic receptor stimulation or cholinergic receptor stimulation [10], which warrants further future investigation.

It is necessary to highlight these limitations, they nevertheless do not affect our conclusions on the underlying pacemaking mechanisms of engineered bio-pacemaker cells, especially regarding the reciprocal interaction of I_{K1} and I_f for a robust bio-pacemaker in modified VMs.

Supporting information

S1 Fig. I-V relation of I_{K1} and I_f with different expression level. S_{K1} and S_f are defined as scaling factors used to simulate the change of I_{K1} and I_f expression level. (A) The I-V curve of I_{K1} with S_{K1} of 1, 0.4, 0.1 that gives I_{K1} densities in the I-V curve at -80 mV 0.99, 0.396 and 0.099 pA/pF respectively. (B) The I-V curve of I_f with S_f of 1, 5, 10 that gives I_f densities in the I-V curve at -80 mV -0.63, -3.15 and -6.3 pA/pF respectively.
(TIF)

S2 Fig. Change of diastolic depolarizing rate with the increase of I_f density. (A) Definition of diastolic depolarizing rate. MDP: maximum diastolic potential; t_1 : the time when membrane potential is MDP; t_2 : the time when potential arrives -55 mV (i.e., around the activation potential of the I_{CaL}). (B) Change of diastolic depolarizing rate with the increase of I_f density from 0 to -6.3 pA/pF when I_{K1} density at -80 mV is at 0.05 pA/pF.
(TIF)

S3 Fig. Ca dynamic of the transient and bursting pacemaking behaviour. (A) Na^+/Ca^{2+} exchange current (I_{NaCa}) during the entire simulating period of 800 s with the current densities of (I_{K1} , I_f) at (0.297 pA/pF, -1.89 pA/pF). (B-D) Na^+/Ca^{2+} exchange current (I_{NaCa}), Ca^{2+} concentration in sarcoplasmic reticulum ($[Ca^{2+}]_{SR}$) and leakage current from SR to cytoplasm (I_{leak}) during the entire simulating period of 800 s with the current densities of (I_{K1} , I_f) at (0.297 pA/pF, -2.52 pA/pF).
(TIF)

S4 Fig. Transient spontaneous pacemaking behaviour. Membrane potential (V) during the entire simulation period of 400 s with the current densities of (I_{K1} , I_f) at (0.178 pA/pF, -0.63 pA/pF).
(TIF)

S5 Fig. Persistent pacemaking activity with periodically incomplete depolarization at different densities of I_{K1} . (A-B) Membrane potential (V) with the current densities of (I_{K1} , I_f) at (0.297 pA/pF, -3.15 pA/pF) and (0.277 pA/pF, -3.15 pA/pF) during simulating time course of 360–370 s.
(TIF)

S6 Fig. Positive effect of I_f on pacemaking ability. (A-F) The membrane potential (V), intracellular Na^+ concentration ($[Na^+]_i$), “funny” current (I_f), intracellular Ca^{2+} concentration ($[Ca^{2+}]_i$), inward rectifier potassium channel current (I_{K1}) and Na^+/Ca^{2+} exchange current (I_{NaCa}) during simulating time course of 400–403 s when the current densities of (I_{K1} , I_f) are at (0.05 pA/pF, 0 pA/pF) and (0.05 pA/pF, -0.63 pA/pF) (dotted and solid line respectively). (Inset A-B) Expanded plots of $[Na^+]_i$ traces for the time course marked by the horizontal brackets with asterisks in (B). (Inset C) The change of $[Ca^{2+}]_i$ with simulating time course of 0–100 s.
(TIF)

S7 Fig. Positive effect of incorporating I_{CaL} on quiet I_{K1}/I_f pacemaker model. (A-F) Membrane potential (V), intracellular Ca^{2+} concentration ($[Ca^{2+}]_i$), Ca^{2+} concentration in sarcoplasmic reticulum ($[Ca^{2+}]_{SR}$), Na^+/Ca^{2+} exchange current (I_{NaCa}), L-type calcium channel current (I_{CaL}) and T-type calcium channel current (I_{CaT}) with the current densities of (I_{K1} , I_f) at (0.297 pA/pF, -0.63 pA/pF) during the simulating period of 0–20 s.
(TIF)

S8 Fig. Side effect of incorporating I_{CaL} on stable I_{K1}/I_f pacemaker model. (A) Membrane potential (V) during the simulating period of 300–302 s. (B–H) Membrane potential (V), intracellular Ca^{2+} concentration ($[Ca^{2+}]_i$), Ca^{2+} concentration in sarcoplasmic reticulum ($[Ca^{2+}]_{SR}$), Na^+/Ca^{2+} exchange current (I_{NaCa}), L-type calcium channel current (I_{CaL}), Na^+/K^+ pumping current (I_{NaK}), fast sodium current (I_{Na}) and “funny” current (I_f) with the current densities of (I_{K1} , I_f) at (0.099 pA/pF, -0.63 pA/pF) during the simulating period of 0–20 s. (TIF)

S1 Text. Prolonged cycle length at greater I_f density.

(DOC)

S2 Text. Model-dependence test.

(DOC)

S1 Code. Biological pacemaker cell model.

(CPP)

Author Contributions

Conceptualization: Henggui Zhang.

Data curation: Yacong Li.

Formal analysis: Yacong Li, Jules C. Hancox, Henggui Zhang.

Funding acquisition: Henggui Zhang.

Investigation: Yacong Li.

Methodology: Yacong Li, Qince Li, Henggui Zhang.

Project administration: Kuanquan Wang, Henggui Zhang.

Resources: Kuanquan Wang, Henggui Zhang.

Software: Yacong Li, Henggui Zhang.

Supervision: Kuanquan Wang, Henggui Zhang.

Validation: Yacong Li.

Visualization: Yacong Li, Henggui Zhang.

Writing – original draft: Yacong Li.

Writing – review & editing: Jules C. Hancox, Henggui Zhang.

References

1. Cohen IS, Brink PR, Robinson RB, Rosen MR. The why, what, how and when of biological pacemakers. *Nat Clin Pract Card.* 2005; 2(8):374–5. <https://doi.org/10.1038/ncpcardio0276> PMID: 16119693
2. Rosen MR. Gene Therapy and Biological Pacing. *New Engl J Med.* 2014; 371(12):1158–9. <https://doi.org/10.1056/NEJMcibr1408897> PMID: 25229921
3. Rosen MR, Brink PR, Cohen IS, Robinson RB. Cardiac pacing: from biological to electronic. . . to biological? *Circ Arrhythm Electrophysiol.* 2008; 1(1):54–61. <https://doi.org/10.1161/CIRCEP.108.764621> PMID: 19808394
4. Rosen MR, Robinson RB, Brink PR, Cohen IS. The road to biological pacing. *Nature reviews Cardiol.* 2011; 8(11):656–66. <https://doi.org/10.1038/nrcardio.2011.120> PMID: 21844918
5. Wilders R, Verheijck EE, Kumar R, Goolsby WN, van Ginneken AC, Joyner RW, et al. Model clamp and its application to synchronization of rabbit sinoatrial node cells. *Am J Physiol.* 1996; 271(5 Pt 2):H2168–82. <https://doi.org/10.1152/ajpheart.1996.271.5.H2168> PMID: 8945938

6. Kapoor N, Galang G, Marban E, Cho HC. Transcriptional suppression of connexin43 by TBX18 undermines cell-cell electrical coupling in postnatal cardiomyocytes. *J Biol Chem*. 2011; 286(16):14073–9. <https://doi.org/10.1074/jbc.M110.185298> PMID: 21205823
7. Freudenberger RS, Wilson AC, Lawrence-Nelson J, Hare JM, Kostis JB. Permanent pacing is a risk factor for the development of heart failure. *American Journal of Cardiology*. 2005; 95(5):671–4. <https://doi.org/10.1016/j.amjcard.2004.10.049> PMID: 15721119
8. Cingolani E, Goldhaber JI, Marban E. Next-generation pacemakers: from small devices to biological pacemakers. *Nature reviews Cardiology*. 2018; 15(3):139–50. <https://doi.org/10.1038/nrcardio.2017.165> PMID: 29143810
9. Shlapakova IN, Nearing BD, Lau DH, Boink GJJ, Danilo P, Kryukova Y, et al. Biological pacemakers in canines exhibit positive chronotropic response to emotional arousal. *Heart Rhythm*. 2010; 7(12):1835–40. <https://doi.org/10.1016/j.hrthm.2010.08.004> PMID: 20708103
10. Kapoor N, Liang WB, Marban E, Cho HC. Direct conversion of quiescent cardiomyocytes to pacemaker cells by expression of Tbx18. *Nat Biotechnol*. 2013; 31(1):54–+. <https://doi.org/10.1038/nbt.2465> PMID: 23242162
11. Miake J, Marban E, Nuss HB. Functional role of inward rectifier current in heart probed by Kir2.1 overexpression and dominant-negative suppression. *J Clin Invest*. 2003; 111(10):1529–36. <https://doi.org/10.1172/JCI17959> PMID: 12750402
12. Hu YF, Dawkins JF, Cho HC, Marban E, Cingolani E. Biological pacemaker created by minimally invasive somatic reprogramming in pigs with complete heart block. *Sci Transl Med*. 2014; 6(245). <https://doi.org/10.1126/scitranslmed.3008681> PMID: 25031269
13. Zhou YF, Yang XJ, Li HX, Han LH, Jiang WP. Mesenchymal stem cells transfected with HCN2 genes by LentiV can be modified to be cardiac pacemaker cells. *Med Hypotheses*. 2007; 69(5):1093–7. <https://doi.org/10.1016/j.mehy.2007.02.032> PMID: 17449188
14. Gorabi AM, Hajighasemi S, Tafti HA, Atashi A, Soleimani M, Aghdami N, et al. TBX18 transcription factor overexpression in human-induced pluripotent stem cells increases their differentiation into pacemaker-like cells. *Journal of cellular physiology*. 2019; 234(2):1534–46. <https://doi.org/10.1002/jcp.27018> PMID: 30078203
15. Noble D. The surprising heart: a review of recent progress in cardiac electrophysiology. *The Journal of physiology*. 1984; 353:1–50. <https://doi.org/10.1113/jphysiol.1984.sp015320> PMID: 6090637
16. DiFrancesco D. The contribution of the 'pacemaker' current (if) to generation of spontaneous activity in rabbit sino-atrial node myocytes. *The Journal of physiology*. 1991; 434:23–40. <https://doi.org/10.1113/jphysiol.1991.sp018457> PMID: 2023118
17. DiFrancesco D. The role of the funny current in pacemaker activity. *Circ Res*. 2010; 106(3):434–46. <https://doi.org/10.1161/CIRCRESAHA.109.208041> PMID: 20167941
18. Mesirca P, Torrente AG, Mangoni ME. T-type channels in the sino-atrial and atrioventricular pacemaker mechanism. *Pflugers Arch*. 2014; 466(4):791–9. <https://doi.org/10.1007/s00424-014-1482-6> PMID: 24573175
19. Guo J, Ono K, Noma A. A sustained inward current activated at the diastolic potential range in rabbit sino-atrial node cells. *The Journal of physiology*. 1995; 483 (Pt 1):1–13. <https://doi.org/10.1113/jphysiol.1995.sp020563> PMID: 7776225
20. Zaritsky JJ, Redell JB, Tempel BL, Schwarz TL. The consequences of disrupting cardiac inwardly rectifying K⁺ current (I-K1) as revealed by the targeted deletion of the murine Kir2.1 and Kir2.2 genes. *J Physiol-London*. 2001; 533(3):697–710. <https://doi.org/10.1111/j.1469-7793.2001.101-1-00697.x> PMID: 11410627
21. Miake J, Marban E, Nuss HB. Gene therapy—Biological pacemaker created by gene transfer. *Nature*. 2002; 419(6903):132–3. <https://doi.org/10.1038/419132b> PMID: 12226654
22. Qu JH, Barbuti A, Protas L, Santoro B, Cohen IS, Robinson RB. HCN2 overexpression in newborn and adult ventricular myocytes—Distinct effects on gating and excitability. *Circ Res*. 2001; 89(1):E8–E14. <https://doi.org/10.1161/hh1301.094395> PMID: 11440985
23. Qu JH, Plotnikov AN, Danilo P, Shlapakova I, Cohen IS, Robinson RB, et al. Expression and function of a biological pacemaker in canine heart. *Circulation*. 2003; 107(8):1106–9. <https://doi.org/10.1161/01.cir.0000059939.97249.2c> PMID: 12615786
24. Plotnikov AN, Sosunov EA, Qu JH, Shlapakova IN, Anyukhovskiy EP, Liu LL, et al. Biological pacemaker implanted in canine left bundle branch provides ventricular escape rhythms that have physiologically acceptable rates. *Circulation*. 2004; 109(4):506–12. <https://doi.org/10.1161/01.CIR.0000114527.10764.CC> PMID: 14734518
25. Ionta V, Liang WB, Kim EH, Rafie R, Giacomello A, Marban E, et al. SHOX2 Overexpression Favors Differentiation of Embryonic Stem Cells into Cardiac Pacemaker Cells, Improving Biological Pacing

- Ability. *Stem Cell Rep.* 2015; 4(1):129–42. <https://doi.org/10.1016/j.stemcr.2014.11.004> PMID: 25533636
26. Xue T, Cho HC, Akar FG, Tsang SY, Jones SP, Marban E, et al. Functional integration of electrically active cardiac derivatives from genetically engineered human embryonic stem cells with quiescent recipient ventricular cardiomyocytes—Insights into the development of cell-based pacemakers. *Circulation.* 2005; 111(1):11–20. <https://doi.org/10.1161/01.CIR.0000151313.18547.A2> PMID: 15611367
 27. Kehat I, Khimovich L, Caspi O, Gepstein A, Shofti R, Arbel G, et al. Electromechanical integration of cardiomyocytes derived from human embryonic stem cells. *Nat Biotechnol.* 2004; 22(10):1282–9. <https://doi.org/10.1038/nbt1014> PMID: 15448703
 28. Bruzauskaite I, Bironaite D, Bagdonas E, Skeberdis VA, Denkovskij J, Tamulevicius T, et al. Relevance of HCN2-expressing human mesenchymal stem cells for the generation of biological pacemakers. *Stem Cell Res Ther.* 2016;7. <https://doi.org/10.1186/s13287-015-0271-2> PMID: 26753925
 29. Zhang H, Li SC, Qu D, Li BL, He B, Wang C, et al. Autologous biological pacing function with adrenergic-responsiveness in porcine of complete heart block. *Int J Cardiol.* 2013; 168(4):3747–51. <https://doi.org/10.1016/j.ijcard.2013.06.012> PMID: 23835270
 30. Planat-Benard V, Menard C, Andre M, Puceat M, Perez A, Garcia-Verdugo JM, et al. Spontaneous cardiomyocyte differentiation from adipose tissue stroma cells. *Circ Res.* 2004; 94(2):223–9. <https://doi.org/10.1161/01.RES.0000109792.43271.47> PMID: 14656930
 31. Choi YS, Dusting GJ, Stubbs S, Arunothayaraj S, Han XL, Collas P, et al. Differentiation of human adipose-derived stem cells into beating cardiomyocytes. *J Cell Mol Med.* 2010; 14(4):878–89. <https://doi.org/10.1111/j.1582-4934.2010.01009.x> PMID: 20070436
 32. Chen L, Deng ZJ, Zhou JS, Ji RJ, Zhang X, Zhang CS, et al. Tbx18-dependent differentiation of brown adipose tissue-derived stem cells toward cardiac pacemaker cells. *Mol Cell Biochem.* 2017; 433(1–2):61–77. <https://doi.org/10.1007/s11010-017-3016-y> PMID: 28382491
 33. Chauveau S, Anyukhovskiy EP, Ben-Ari M, Naor S, Jiang YP, Danilo P, et al. Induced Pluripotent Stem Cell-Derived Cardiomyocytes Provide In Vivo Biological Pacemaker Function. *Circ-Arrhythmia Elec.* 2017; 10(5). <https://doi.org/10.1161/CIRCEP.116.004508> PMID: 28500172
 34. Gorabi AM, Hajighasemi S, Khori V, Soleimani M, Rajaei M, Rabbani S, et al. Functional biological pacemaker generation by T-Box18 protein expression via stem cell and viral delivery approaches in a murine model of complete heart block. *Pharmacological research.* 2019; 141:443–50. <https://doi.org/10.1016/j.phrs.2019.01.034> PMID: 30677516
 35. Kleber AG, Rudy Y. Basic mechanisms of cardiac impulse propagation and associated arrhythmias. *Physiol Rev.* 2004; 84(2):431–88. <https://doi.org/10.1152/physrev.00025.2003> PMID: 15044680
 36. Potapova I, Plotnikov A, Lu ZJ, Danilo P, Valiunas V, Qu JH, et al. Human mesenchymal stem cells as a gene delivery system to create cardiac pacemakers. *Circ Res.* 2004; 94(7):952–9. <https://doi.org/10.1161/01.RES.0000123827.60210.72> PMID: 14988226
 37. Plotnikov AN, Shlapakova I, Szabolcs MJ, Danilo P, Lorell BH, Potapova IA, et al. Xenografted adult human mesenchymal stem cells provide a platform for sustained biological pacemaker function in canine heart. *Circulation.* 2007; 116(7):706–13. <https://doi.org/10.1161/CIRCULATIONAHA.107.703231> PMID: 17646577
 38. Saito Y, Nakamura K, Yoshida M, Sugiyama H, Ohe T, Kurokawa J, et al. Enhancement of Spontaneous Activity by HCN4 Overexpression in Mouse Embryonic Stem Cell-Derived Cardiomyocytes—A Possible Biological Pacemaker. *Plos One.* 2015; 10(9). <https://doi.org/10.1371/journal.pone.0138193> PMID: 26384234
 39. Cho HC, Kashiwakura Y, Marban E. Creation of a biological pacemaker by cell fusion. *Circ Res.* 2007; 100(8):1112–5. <https://doi.org/10.1161/01.RES.0000265845.04439.78> PMID: 17395872
 40. Azene EM, Xue T, Marban E, Tomaselli GF, Li RA. Non-equilibrium behaviour of HCN channels: Insights into the role of HCN channels in native and engineered pacemakers. *Cardiovasc Res.* 2005; 67(2):263–73. <https://doi.org/10.1016/j.cardiores.2005.03.006> PMID: 16005302
 41. Lieu DK, Chan YC, Lau CP, Tse HF, Siu CW, Li RA. Overexpression of HCN-encoded pacemaker current silences bioartificial pacemakers. *Heart Rhythm.* 2008; 5(9):1310–7. <https://doi.org/10.1016/j.hrthm.2008.05.010> PMID: 18693074
 42. Kuwabara Y, Kuwahara K, Takano M, Kinoshita H, Arai Y, Yasuno S, et al. Increased Expression of HCN Channels in the Ventricular Myocardium Contributes to Enhanced Arrhythmicity in Mouse Failing Hearts. *J Am Heart Assoc.* 2013; 2(3). <https://doi.org/10.1161/JAHA.113.000150> PMID: 23709563
 43. Sun Y, Timofeyev V, Dennis A, Bektik E, Wan XP, Laurita KR, et al. A Singular Role of I-K1 Promoting the Development of Cardiac Automaticity during Cardiomyocyte Differentiation by I-K1-Induced Activation of Pacemaker Current. *Stem Cell Rev Rep.* 2017; 13(5):631–43. <https://doi.org/10.1007/s12015-017-9745-1> PMID: 28623610

44. Yang M, Zhang GG, Wang T, Wang X, Tang YH, Huang H, et al. TBX18 gene induces adipose-derived stem cells to differentiate into pacemaker-like cells in the myocardial microenvironment. *Int J Mol Med*. 2016; 38(5):1403–10. <https://doi.org/10.3892/ijmm.2016.2736> PMID: 27632938
45. Chen K, Zuo D, Wang SY, Chen H. Kir2 inward rectification-controlled precise and dynamic balances between Kir2 and HCN currents initiate pacemaking activity. *FASEB J*. 2018; 32(6):3047–57. <https://doi.org/10.1096/fj.201701260R> PMID: 29401592
46. Silva J, Rudy Y. Mechanism of pacemaking in I-K1-downregulated myocytes. *Circ Res*. 2003; 92(3):261–3. <https://doi.org/10.1161/01.res.0000057996.20414.c6> PMID: 12595336
47. Kurata Y, Hisatome I, Matsuda H, Shibamoto T. Dynamical mechanisms of pacemaker generation in I-K1-downregulated human ventricular myocytes: Insights from bifurcation analyses of a mathematical model. *Biophys J*. 2005; 89(4):2865–87. <https://doi.org/10.1529/biophysj.105.060830> PMID: 16040746
48. Tong WC, Holden AV. Induced pacemaker activity in virtual mammalian ventricular cells. *Lect Notes Comput Sc*. 2005; 3504:226–35.
49. Kurata Y, Matsuda H, Hisatome I, Shibamoto T. Roles of hyperpolarization-activated current I_f in sinoatrial node pacemaking: insights from bifurcation analysis of mathematical models. *American journal of physiology Heart and circulatory physiology*. 2010; 298(6):H1748–60. <https://doi.org/10.1152/ajpheart.00729.2009> PMID: 20363885
50. Kurata Y, Matsuda H, Hisatome I, Shibamoto T. Effects of pacemaker currents on creation and modulation of human ventricular pacemaker: theoretical study with application to biological pacemaker engineering. *American journal of physiology Heart and circulatory physiology*. 2007; 292(1):H701–18. <https://doi.org/10.1152/ajpheart.00426.2006> PMID: 16997892
51. Maltsev VA, Lakatta EG. Numerical models based on a minimal set of sarcolemmal electrogenic proteins and an intracellular Ca^{2+} clock generate robust, flexible, and energy-efficient cardiac pacemaking. *Journal of molecular and cellular cardiology*. 2013; 59:181–95. <https://doi.org/10.1016/j.yjmcc.2013.03.004> PMID: 23507256
52. ten Tusscher KH, Panfilov AV. Alternans and spiral breakup in a human ventricular tissue model. *American journal of physiology Heart and circulatory physiology*. 2006; 291(3):H1088–100. <https://doi.org/10.1152/ajpheart.00109.2006> PMID: 16565318
53. Fabbri A, Fantini M, Wilders R, Severi S. Computational analysis of the human sinus node action potential: model development and effects of mutations. *The Journal of physiology*. 2017; 595(7):2365–96. <https://doi.org/10.1113/JP273259> PMID: 28185290
54. ten Tusscher KHWJ, Noble D, Noble PJ, Panfilov AV. A model for human ventricular tissue. *Am J Physiol-Heart C*. 2004; 286(4):H1573–H89.
55. Zhang H, Butters T, Adeniran I, Higham J, Holden AV, Boyett MR, et al. Modeling the chronotropic effect of isoprenaline on rabbit sinoatrial node. *Frontiers in physiology*. 2012; 3:241. <https://doi.org/10.3389/fphys.2012.00241> PMID: 23060799
56. Whittaker DG, Ni H, Benson AP, Hancox JC, Zhang H. Computational Analysis of the Mode of Action of Disopyramide and Quinidine on hERG-Linked Short QT Syndrome in Human Ventricles. *Frontiers in physiology*. 2017; 8:759. <https://doi.org/10.3389/fphys.2017.00759> PMID: 29085299
57. O'Hara T, Virag L, Varro A, Rudy Y. Simulation of the undiseased human cardiac ventricular action potential: model formulation and experimental validation. *PLoS computational biology*. 2011; 7(5):e1002061. <https://doi.org/10.1371/journal.pcbi.1002061> PMID: 21637795
58. Irnich W, de Bakker JM, Bisping HJ. Electromagnetic interference in implantable pacemakers. *Pacing Clin Electrophysiol*. 1978; 1(1):52–61. <https://doi.org/10.1111/j.1540-8159.1978.tb03441.x> PMID: 83621
59. Plaster NM, Tawil R, Tristani-Firouzi M, Canun S, Bendahhou S, Tsunoda A, et al. Mutations in Kir2.1 cause the developmental and episodic electrical phenotypes of Andersen's syndrome. *Cell*. 2001; 105(4):511–9. [https://doi.org/10.1016/s0092-8674\(01\)00342-7](https://doi.org/10.1016/s0092-8674(01)00342-7) PMID: 11371347
60. Zhang H, Tong W-C, Garratt C, Holden A. Stability of genetically engineered cardiac pacemaker—role of intracellular Ca^{2+} handling. *Comput Cardiol*2005. p. 969–72.
61. Boink GJJ, Duan L, Nearing BD, Shlapakova IN, Sosunov EA, Anyukhovskiy EP, et al. HCN2/SKM1 Gene Transfer Into Canine Left Bundle Branch Induces Stable, Autonomically Responsive Biological Pacing at Physiological Heart Rates. *J Am Coll Cardiol*. 2013; 61(11):1192–201. <https://doi.org/10.1016/j.jacc.2012.12.031> PMID: 23395072
62. Boink GJ, Nearing BD, Shlapakova IN, Duan L, Kryukova Y, Bobkov Y, et al. Ca^{2+} -stimulated adenylyl cyclase AC1 generates efficient biological pacing as single gene therapy and in combination with HCN2. *Circulation*. 2012; 126(5):528–36. <https://doi.org/10.1161/CIRCULATIONAHA.111.083584> PMID: 22753192

63. Ono K, Iijima T. Pathophysiological significance of T-type Ca^{2+} channels: properties and functional roles of T-type Ca^{2+} channels in cardiac pacemaking. *J Pharmacol Sci.* 2005; 99(3):197–204. <https://doi.org/10.1254/jphs.fmj05002x2> PMID: 16272791
64. Verkerk AO, Wilders R, van Borren MM, Peters RJ, Broekhuis E, Lam K, et al. Pacemaker current (I_f) in the human sinoatrial node. *Eur Heart J.* 2007; 28(20):2472–8. <https://doi.org/10.1093/eurheartj/ehm339> PMID: 17823213
65. Pan L, Lines GT, Maleckar MM, Aslak T. Mathematical models of cardiac pacemaking function. *Frontiers in Physics.* 2013; 1.
66. Maltsev VA, Lakatta EG. Synergism of coupled subsarcolemmal Ca^{2+} clocks and sarcolemmal voltage clocks confers robust and flexible pacemaker function in a novel pacemaker cell model. 2009; 296(3): H594–615.
67. Sirenko S, Maltsev VA, Maltseva LA, Yang D, Lukyanenko Y, Vinogradova TM, et al. Sarcoplasmic reticulum Ca^{2+} cycling protein phosphorylation in a physiologic Ca^{2+} milieu unleashes a high-power, rhythmic Ca^{2+} clock in ventricular myocytes: relevance to arrhythmias and bio-pacemaker design. *Journal of molecular and cellular cardiology.* 2014; 66:106–15. <https://doi.org/10.1016/j.yjmcc.2013.11.011> PMID: 24274954